PREPARATION, CHARACTERISATION OF MIXED METAL OXIDE NANOCOMPOSITES OF Ce / Mo / Ti FOR ELECTROCHEMICAL APPLICATION

UTHIRA SELVI. B*[a], Dr. JESSICA FERNANDO[b]

Article History: **Received**: 29.05.2022 **Revised**: 28.06.2022 **Accepted**: 11.07.2022

Abstract: Transition metal oxides are apt materials for energy storage devices due to their high theoretical specific capacity, high thermal stability and abundance. The synthesis of mixed metal oxide (MMO) nanocomposites of Ce/Mo/Ti and characterization using UV, FTIR, field emission scanning electron microscopy and XRD to investigate the optical and structural properties. UV-Vis studies of the prepared nanocomposites show that the absorption is aspect to the transfer of electrons from the valence band to the conduction band. FTIR analysis confirms the presence of metal oxides by the corresponding metal oxide stretching vibrations. The particle size of Ce/Mo/Ti MMO nanocomposite is in the range of 10.93 nm – 48.95 nm and has uniform spherical particles from FESEM images. Cyclic voltammetric studies of Ce/Mo/Ti MMO shows that the calculated specific capacitance value is 143 F/g at pH 9 due to the uniform nanostructure.

Keywords: Nanocomposites, MMO, FTIR, UV-Vis, XRD, EIS, FESEM

[a]. Research Scholar (19112232032001), PG & Research Department of Chemistry, V.O.Chidambaram College, Tuticorin - 628008, Affiliated to Manonmaniam Sundaranar University, Abishekapatti, Tirunelveli-627012, Tamilnadu, India.
[b]. Assistant Professor, PG and Research Department of Chemistry, V.O.Chidambaram College, Thoothukudi - 628008, Affiliated to Manonmaniam Sundaranar University, Abishekapatti, Tirunelveli-627 012, Tamilnadu, India.

*Corresponding Author

Email: uthiraselvi14@gmail.com.

DOI: 10.31838/ecb/2022.11.04.010

INTRODUCTION

Recently, the synthesis of mixed metal oxide nanocomposites has emerged as an attractive research area in material chemistry since the morphology and the size of the nanocomposites. A rare earth oxide - cerium oxide (CeO_2) is attain a lot of focus due to its low cost, very low toxicity, surplus availability, highly reversible oxidation states (3^+ /4^+), no phase change at operational conditions (1-9). Among metal oxides, two combination of metal oxides such as metal tungstates and metal molybdates have attracted much attention in energy storage studies (10-12). Metal molybdate is one of the most up-to-date materials in the study of supercapacitive materials with tremendous electrochemical performance and high specific capacitance [13–15]. Cerium molybdate is an essential yellow inorganic substance with monoclinic crystalline structure that has been analysed by the scientific community due to its photonics properties and photoluminescent. Owing to the unsteadiness of the cerium ion at high temperatures, there is certain difficulty in synthesizing a well-crystallized singlephase cerium molybdate with its appropriate crystalline structure, monoclinic symmetry (16). Hence, the synthesis method has an important role in the structure of the material, and consequently in its electronic properties. Transition metal-based molybdates (M = Zn, Mn, Mg, Sr, Ba, Ni, Co, Pb, Ca, Cd, Cu etc.,) have been recognized and notably applied in varied fields such as photoluminescence, magnetic properties, optical fibers, photocatalyst, illumination, lasers, phytoremediation, catalyst, supercapacitors, humidity sensor, Li-ion storage batteries and scintillation crystal (17–31). In recent times, several metal molybdates with different morphologies, properties and size have been synthesized nanorods, nanowires, superstructures, doughnut-shaped microstructures, nest like nanostructures, nanoplates, dendrites, thin film, nanopowders and flower-like mesocrystal and so on (32–36, 30). Rare earth molybdates are important because of their application in phosphors, catalysts and thermal expansion materials (37) and has various properties like corrosion inhibitor, good catalytic-convertor and high photostability.

Despite their promising potential applications and unique properties, to the best of our knowledge, there are some investigations on the synthesis of cerium molybdate based nanocomposites. In this paper, we reported a synthesis of Ce/Mo/Ti oxide nanocomposites and its optical property, characterization and their structural morphology.

MATERIAL AND METHODS

Materials: Ammonium ceric nitrate ($(NH_4)_2Ce(NO_3)_6$), Ammonium molybdate ($(NH_4)_6Mo_7O_{24}$), Titanium tetra chloride ($TiCl_4$), Sodium docusate ($C_{20}H_{37}NaO_7S$) and Sodium hydroxide were procured from Merck, India. Double distilled water was used in synthesis procedure. All chemicals were used as supplied without further purification.

Synthesis of (Ce/Mo/Ti) MMO nanocomposite: 0.1 N 100mL solution of Ammonium ceric nitrate ($(NH_4)_2Ce(NO_3)_6$) and Ammonium molybdate ($(NH_4)_6Mo_7O_{24}$) were prepared by dissolving separately in deionised water under constant stirring for 15 min and 0.1 N 100mL solution of Titanium tetra chloride ($TiCl_4$) was prepared by slowly added to the distilled water at 5◦C. When $TiCl_4$ dissolved in distilled water, the heat was produced due to exothermic reaction and the formation of orthotitanic acid [$Ti(OH)_4$]. To prevent for the formation of orthotitanic acid , 5 ml of hydrochloric acid (35% HCl) per 100 ml of distilled water was added and stirred for 15 min., The three solutions were mixed together. A saturated solution of sodium docusate $C_{20}H_{37}NaO_7S$ surfactant was added dropwise to the mixture. Finally, NaOH was added until the complete gel was formed. This solution was magnetically stirred for 4hrs. The particles were separated by ultracentrifugation and washed with water. The final product was dried, ground and annealed at 500 °C for 4 h to remove volatile impurities.

Characterization: UV-Vis spectra of the samples were taken using JASCO-V 530 dual beam spectrophotometer in the wavelength region 200 to 900 nm with a scanning speed of 400 nm/min. The prepared nanocomposite was characterized by KBr disks performed on a Thermo Scientific Nicolet iS5 FT-IR spectrometer in the frequency range of 400 to 4000 cm^{-1}. X-ray diffraction (XRD) helps to find the geometry and shape of a molecule using X-rays. The morphology of the prepared composite was determined using field emission scanning electron microscope (FESEM) and energy dispersive X-ray (EDS) was used to confirm the element composition in the composite. The CH-Instrument of electrochemical workstation (mode-650 c) is used for cyclic voltammetry studies.

RESULTS AND DISCUSSION

UV-Vis spectra: Characterization of as prepared MMO nanocomposite was carried out by UV–vis spectroscopy. UV-Vis spectra are recorded in the region 200 to 900 nm shown in Figure 1. The bandgap energies of the prepared nanocomposite has been resolved using the Tauc-equation [38]

$$(\alpha h\nu)^{1/n}=A(h\nu - Eg) \qquad \text{-------(1)}$$

where α is the absorption co-efficient, Eg is the band gap energy, A is a constant and n = 1 for the direct band gap. For allowed direct transition n=2, a graph between $(\alpha h\nu)^2$ and hν is plotted, extrapolation of the straight line to $(\alpha h\nu)^2$ axis shows the value of the band gap energy. Fig.1 shows the UV–vis spectra of Ce/Mo/Ti oxide nanocomposite. The peaks at 237 nm shows maximum absortion peaks it may be due to π conjuagation system transition of oxide nanoparticles [39]. From the Tauc plot Ultraviolet-visible absorption spectroscopy exposes a characteristic optical band gap of 4.3 eV.

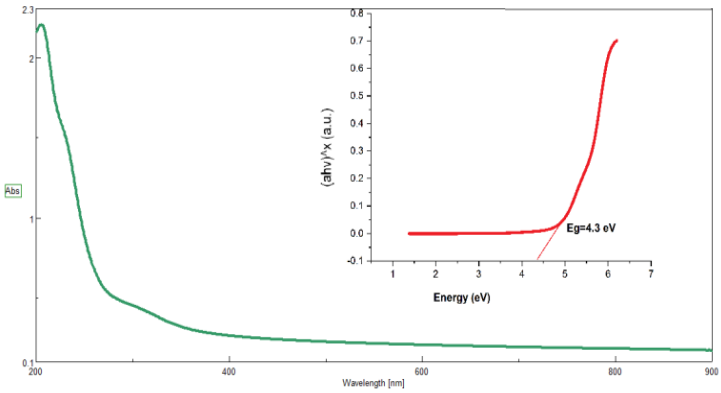

Figure 1. UV-Vis pattern of (Ce/Mo/Ti) oxide nanocomposites

The UV-Vis-NIR spectra of the ZnSe/EVA nanocomposites are recorded in the region 200 to 2000 nm are shown in Figure 5. The bandgap of the prepared nanocomposites has been determined using the Tauc-relation [18]

FT IR spectra

The Fourier Transform Infrared Spectroscopy (FTIR) identifies the chemical bonds in a molecule by producing an infrared absorption spectrum. FTIR spectra were recorded for the as prepared nanocomposite in the range 400-4000 cm^{-1} and presented in Fig 2. The spectra of the prepared nanocomposites was observed and identified as the peak at 3420 cm^{-1} is due to O–H stretching of water molecle and also the bands at 1628 cm^{-1} is O–H bending mode of the (Ce/Mo/Ti) oxide. The bands at 2921 assigned to C–H asymmetric and symmetric stretching modes of the sp^3 congregation of the residual organic template, and the corresponding band around 1421 cm^{-1} is due to C–H bending mode. The peaks at 1127 cm^{-1} are featured to the asymmetric stretching of the metal and oxygen framework. The low frequency region bands within the range of 400–800 cm^{-1} corresponding to the lattice vibration modes of M-O and O-M-O (M = Ce, Mo, Ti) [40]. The peak at 1500-1700 cm^{-1} is ascribed to the bending modes of Ti-O-Ti [41]. The vibrational peaks examined between 900 cm^{-1}, is assigned to Mo=O characteristic stretching vibration of the hexagonal phase MoO_3 [42].

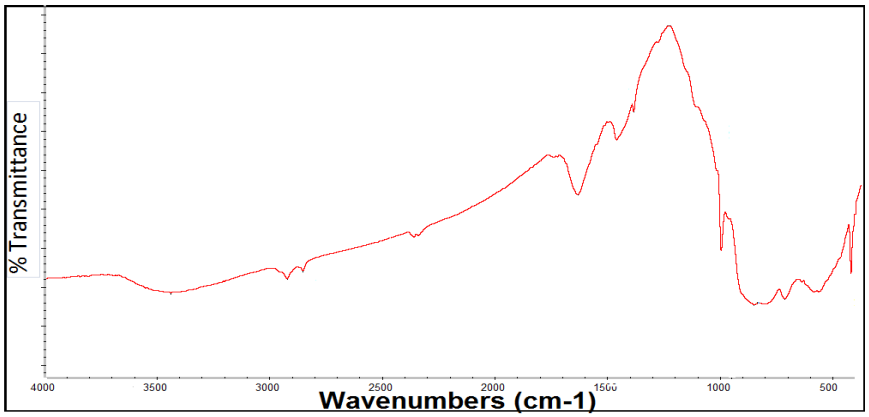

Figure 2. FTIR image of (Ce/Mo/Ti) MMO nanocomposite

XRD: XRD patterns of Ce/Mo/Ti oxide nanocomposites exhibits narrow and sharp diffraction peaks, which denotes the perfect crystallinity. Sample XRD peaks are assigned and distinguishable the single part of the crystal structures. It shows the intense diffraction peaks. The XRD patterns of the (Ce/Mo/Ti) oxide NPs shows the diffraction angle of 2θ values at 19.06°, 28.53°, 33.91°, 39.20°, 39.22°, 46.79° 57.71° and 75.12° are attributed to (100), (200), (110), (130), (300), (140), (002) and (524) planes of h-MoO3 , α- MoO3 (JCPDS card no. 21-0569, 05-0508) respectively [43]. The diffraction peaks of 2θ values for 48.58°, 53.62° and 71.62° are due to (220), (222) and (331) planes of CeO_2 (JCPDS card no. 34-0394) respectively [44]. The diffraction peaks at 2θ values of 28.02°, 28.68° and 34.08° are assigned to (121), (200) and (110) planes of TiO_2 (JCPDS card no. 21-1272) respectively [45]. From the XRD data the size of the nanoparticles can be calculated by Scherer equation.

Crystallite size = 0.94 x (X-ray wavelength) / βcos θ ---(2)

The average crystal sizes of the metal oxides are determined to be 49.05 nm for samples (Ce/Mo/Ti) oxide nanocomposites . The XRD results indicate the highly crystalline nature of the nancomposite and it has the size within the nanometre.

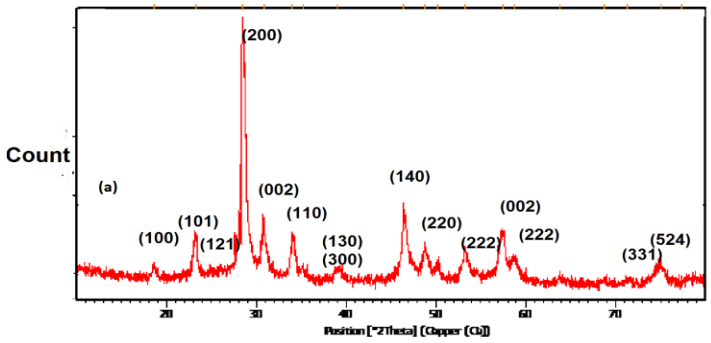

Figure 3. XRD of (Ce/Mo/Ti) oxide nanocomposites

FE-SEM and EDS analysis

The surface morphology and shape of the synthesized MMO of (Ce/Mo/Ti) is used to identify by Scanning electron microscopy (SEM) as shown in Fig 4.(a) (Ce/Mo/Ti) oxide nanocomposites display uniform spherical particles. Evidently, dozens of nano sphere be linked to each other through the centre to form the agglomerated architecture. The particle size of Ce/Mo/Ti MMO nanocomposites is in the range of 10.93 nm – 48.95 nm. It shows a regular network like structure of uniformed sphere which results the lowest particle size. This is may be due to the presence of surfactant used for the preparation of the nanocomposites. The elemental compositions of the (Ce/Mo/Ti) oxide nanocomposites arrays have been investigated by SEM EDS from Fig4.(b). The chemical elements of cerium, molybdenum, titanium, oxygen, and carbon were detected in the (Ce/Mo/Ti) oxide nanocomposites arrays and the survey results confirmed the compositions.

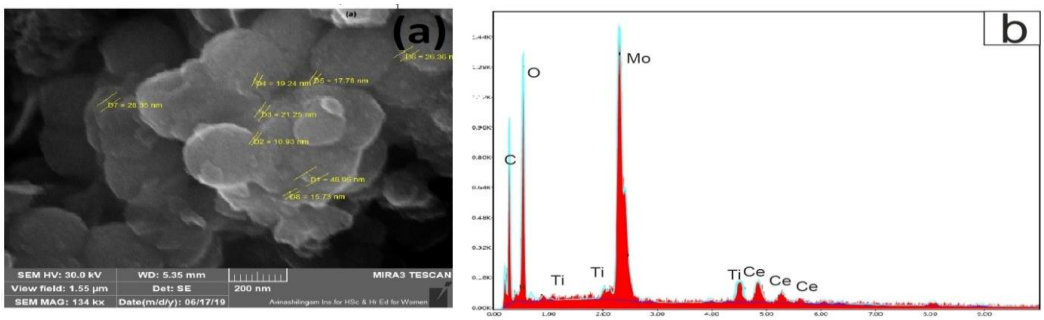

Figure 4. (a)Scanning electron micrograph and (b) EDS of (Ce/Mo/Ti) oxide nanocomposites

Electrochemical measurements:

The electrochemical studies of the composites carried out in a three-electrode cell. Counter electrode is platinum wire, Ag/Ag chloride electrode as a reference electrode and metal oxide nanoparticle coated on ITO (Indium tin oxide) plate was used as working electrode. The impedance measurements was carried out using electrochemical workstation (mode 650C), CH-Instrument, TX, USA. The electrochemical behaviour of the (Ce/MO/Ti) oxide electrode was investigated for pH9.These measurements were performed in the potential range of – 1.6 to 2 V. Fig 5.(a) shows the CV curves of the nanocomposites at various scan rates of 5 mVs^{-1}, 10 mVs^{-1}, 20 mVs^{-1},30 mVs^{-1}, 50 mVs^{-1} and 100 mVs^{-1} for pH 9. The redox peaks in the CVs of the (Ce/MO/Ti) oxide electrode indicates the presence of a Faradic reaction. Charge storage is controlled to the surface of the electrode. However, redox type pseudocapacitance is not restricted to the electrode material surfaces and can also occur in the sub-surface redox active sites [46]. In fact, observing a rapid current response to voltage reversal at the end of each potential indicates the ideal pseudocapacitive behaviour of the prepared composites. From Fig 5(a), the cyclic voltammety curve area increases with increase in scan rate from 5 mVs^{-1} to 100 mVs^{-1} for pH 9 electrolyte. The specific capacitance value is estimated using the following equation (3).

$C_p = A/ 2mk (V_2-V_1)$ ---------- (3)

Where Cp in F/g. A - Area inside CV curve (ΔV), m is the mass of active material, k-scan rate of CV (V/sec) and (V_2-V_1)-total voltage range. Table 1. Shows the Specific capacitance (C_p) values of (Ce/MO/Ti). For low scan rate, the capacitance value is high. The voltage and current increases with increases in scan rate. At lower scan rate of 5 mVs^{-1} the specific current increases which results the decrease in specific capacitance of the nanocomposites from Fig 5(a).

Table 1. Calculated values of specific capacitance

Sample	Scan rate (mVs^{-1})	C_p(F/g)
(Ce/MO/Ti) oxide	5	143
	10	103
	20	90
	30	76
	50	61
	100	36

Table 2. Rct and Cdl values of (Ce/Mo/Ti) oxides

Sample	R_S	Rct(Ωcm2)	Cdl(µFcm^{-2})
(Ce/MO/Ti) oxide	91.12	$3.209x10^4$	$2.648x10^{-6}$

To interpret the performance of the electrode material and the kinetics of the entire electrochemical system of (Ce/Mo/Ti) oxides, EIS is used (Electrochemical Impedance spectroscopy) . From EIS, Fig .5(c) shows the Nyquist plot of both composites measured for Ph 9 solution in three-electrode configuration. Randle's circuit is used to fit impedance data. In Randle's circuit, R_{ct} -charge transfer resistance, R_s- solution resistance, C_{dl}- double layer capacitor, R_p- polarization resistance and it was assumed that the diffusion impedance (W) were both in parallel to the interfacial capacity. This resistance reveals that the electron transfer kinetics of the redox probe at the electrode interface. The double layer capacitance is in parallel with the charge transfer resistance. The charge transfer resistance related with a semicircle in a higher frequency region with a resistance signifies high conductivity of the electrode in both samples and also has very low internal resistance with high-frequency response. This low charge transfer resistance highlights that the MMOs are best for electrochemical applications.

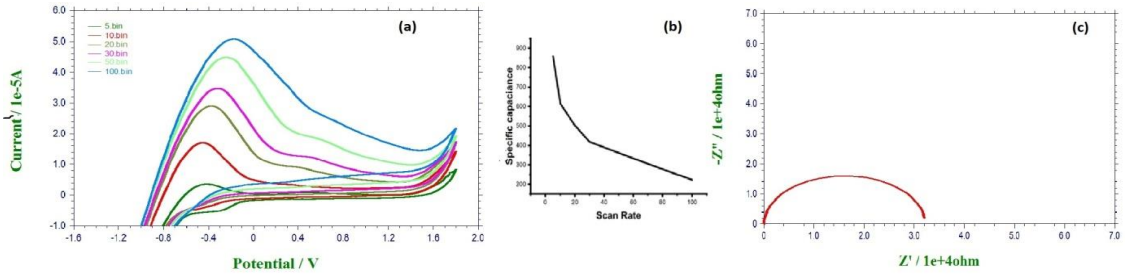

Figure 5. (a) CV curves of (Ce/Mo/Ti) oxide at different scan rates (b) variation of specific capacitance with scanrate (c) Nyquist plot of (Ce/Mo/Ti) oxide electrode material

CONCLUSION

Synthesis of (Ce-Mo-Ti) mixed metal oxide nanocomposite was successfully carried out. They were characterized by spectral studies (UV-Vis and FTIR). The optical properties of the cerium molybdate were studied by UV-Vis spectra and its band gap was calculated as 4.3 eV. SEM confirms Ce/Mo/Ti mixed metal oxide nanocomposite were within the nanometre range and particularly it has 10.93 nm – 28.35 nm ranged sphere shaped aggregated particles. Cyclic voltammetric studies of Ce/Mo/Ti MMO shows that the calculated specific capacitance value is 143 F/g at pH 9. Studies show that the nanocomposite can be used in many fields such as sensors, solar cells, corrosion industry, ceramics, plastics, inorganic pigments in paints, in the field of catalysis and also it can be used as supercapacitor for energy storage devices.

ACKNOWLEDGEMENT

The authors are thankful to PG and Research Department of chemistry, V. O. Chidambaram College, Thoothukudi.

REFERENCES

i. Brezesinski, T.; Wang, J.; Senter, R.; Brezesinski, K.; Dunn, B.; Tolbert, S. H., On the Correlation between Mechanical Flexibility, Nanoscale Structure, and Charge Storage in Periodic Mesoporous CeO2 Thin Films. ACS Nano **2010,** 4 (2), 967-977.

ii. Tao, Y.; Ruiyi, L.; Haiyan, Z.; Zaijun, L., Ceria nanoparticles uniformly decorated on graphene nanosheets with coral-like morphology for high-performance supercapacitors. Materials Research Bulletin **2016,** 78, 163-171.

iii. Trovarelli, A., Catalytic properties of ceria and CeO2-containing materials. Catalysis Reviews **1996,** 38 (4), 439-520.

iv. Heydari, H.; Gholivand, M. B., A novel high-performance supercapacitor based on high-quality CeO2/nitrogen-doped reduced graphene oxide nanocomposite. Applied Physics A **2017,** 123 (3), 187.

v. Karakoti, A.; Singh, S.; Dowding, J. M.; Seal, S.; Self, W. T., Redox-active radical scavenging nanomaterials. Chemical Society Reviews **2010,** 39 (11), 4422-4432.

vi. Kumar, R.; Agrawal, A.; Nagarale, R. K.; Sharma, A., High performance supercapacitors from novel metal-doped ceria-decorated aminated graphene. J. Phys. Chem. C **2016,** 120 (6), 3107-3116.

vii. Corma, A.; Atienzar, P.; García, H.; Chane-Ching, J.-Y., Hierarchically mesostructured doped CeO2 with potential for solar-cell use. Nature materials **2004,** 3 (6), 394-397.

viii. Dezfuli, A. S.; Ganjali, M. R.; Naderi, H. R.; Norouzi, P., A high performance supercapacitor based on a ceria/graphene nanocomposite synthesized by a facile sonochemical method. RSC Advances **2015,** 5 (57), 46050-46058.

ix. Montini, T.; Melchionna, M.; Monai, M.; Fornasiero, P., Fundamentals and catalytic applications of CeO2-based materials. Chemical reviews **2016,** 116 (10), 5987-6041.

x. H. Cao, N. Wu, Y. Liu, S. Wang, W. Du, J. Liu, Facile synthesis of rod-like manganese molybdate crystallines with two-dimensional nanoflakes for supercapacitor application. Electrochim. Acta **225**, 605–613 (2017)

xi. C. Cui, J. Xu, L. Wang, D. Guo, M. Mao, J. Ma, T. Wang, Growth of NiCo2O4@ MnMoO4nanocolumn arrays with superior pseudocapacitors properties. ACS Appl. Mater. Interfaces **8**, 8568–8575 (2016)

xii. H. Wan, J. Jiang, X. Ji, L. Miao, L. Zhang, K. Xu, H. Chen, Y.Ruan, Rapid microwave-assisted synthesis NiMoO4H2O Nanoclusters for supercapacitors. Mater. Lett. **108**, 164–167 (2013)

xiii. Z.S. Wu, G. Zhou, L.C. Yin, W. Ren, F. Li, H.M. Cheng, Graphene / metal oxide composite electrode materials for energy storage. Nano Energy **1**, 107–131 (2012)

xiv. K.A. Yasakau, J. Tedim, M.L. Zheludkevich, R. Drumm, M. Shem, M. Wittmar, M. Veith, M.G.S. Ferreira, Cerium molybdate nanowires for active corrosion protection of aluminum alloys Corros. Sci. **58**, 41–51 (2012)

xv. Y.P. Gao, K.J. Huang, C.X. Zhang, S.S. Song, X. Wu, High performance symmetric supercapacitor based on flower-like zinc molybdate. J. Alloys Compd. **731**, 1151–1158 (2018)

xvi. Brazdil JF. Scheelite: a versatile structural template for selective alkene oxidation catalysts. Catalysis Science & Technology. 2015;5(7):3452-3458.

xvii. R. Sundaram, K. S. Nagaraja, Solid state electrical conductivity and humidity sensing studies on metal molybdate–molybdenum trioxide composites (M = Ni2+, Cu2+ 29 and Pb2+ 30). Sens. Actuators B, 2004, 101, 353–360.

xviii. A. Kumar, J. Kumar, Perspective on europium activated fine-grained metal molybdate phosphors for solid state illumination. J. Mater. Chem, 2011, 21, 3788–3795.

xix. J. H. Ryu, J. W. Yoon, C. S. Lim, W. C. Oh, K. B. Shim, Microwave-assisted synthesis of CaMoO4 nano-powders by a citrate complex method and its photoluminescence property. J. Alloys Compd, 2005, 390, 245–249.

xx. Z. Zhang, Y. Liu, Z. Huang, L. Ren, X. Qi, X. Wei, J. Zhong, Facile hydrothermal synthesis of NiMoO4@CoMoO4 hierarchical nanospheres for supercapacitor applications. Phys ChemChem Phys, 2015, 17, 20795–20804.

xxi. A. S. Nasab, M. Maddahfar, S. M. H. Mashkani, Ce(MoO4)2 nanostructures: Synthesis, characterization, and its photocatalyst application through the ultrasonic method. J. Mol. Liq, 2016, 216, 1–5.

xxii. J. Qu, L. Wang, X. Yuan, Q. Cong, S. S. Guan, Effects of ammonium molybdate on phytoremediation by alfalfa plants and (im)mobilization of toxic metals in soils. Environ. Earth Sci, 2011, 64, 2175–2182.

xxiii. S. Driscoll, U. S. Ozkan, Isotopic Labeling Studies on Oxidative Coupling of Methane over Alkali Promoted Molybdate Catalysts. Stud. Surf. Sci. Catal, 1994, 82, 367–375

xxiv. G. Schwarz, J. Schulze, F. Bittner, T. Eilers, J. Kuper, G. Bollmann, A. Nerlich, H. Brinkmann, R. R. Mendel, The Molybdenum Cofactor Biosynthetic Protein Cnx1 Complements Molybdate-Repairable Mutants, Transfers Molybdenum to the Metal Binding Pterin, and Is Associated with the Cytoskeleton. Plant Cell, 2000, 12, 2455– 2471.

xxv. J. G. Rushbrooke, R. E. Ansorge, Optical fibre readout and performance of small scintillating crystals for a fine-grained gamma detector. Nucl. Instrum. Methods Phys.Res. Sect A, 1989, 280, 83–90

xxvi. Y. Ding, S. H. Yu, C. Liu, Z. A. Zang, 3D Architectures of Iron Molybdate: Phase Selective Synthesis, Growth Mechanism, and Magnetic Properties. Chem. Eur. J, 2007, 13, 746–753

xxvii. M. Shen, X. Zhang, K. Dai, H. Chen, T. Peng, Hierarchical PbMoO4 microspheres: hydrothermal synthesis, formation mechanism and photocatalytic properties. CrystEng Comm, 2013, 15, 1146–1152.

xxviii. V. B. Mikhailik, H. Kraus, Performance of scintillation materials at cryogenic 2 temperatures. Phys. Status Solidi. B, 2010, 247, 1583–1599.

xxix. J. P. Liu, X. T. Huang, Y. Y. Li, Z. K. Li, A general route to thickness-tunable multilayered sheets of sheelite-type metal molybdate and their self-assembled films. J. Mater. Chem, 2007, 17, 2754–2758.

xxx. W. Xiao, J. S. Chen, C. M. Li, R. Xu, X. W. Lou, Synthesis, Characterization, and Lithium Storage Capability of AMoO4 (A = Ni, Co) Nanorods. Chem. Mater, 2010, 22, 746–754.

xxxi. B. Senthilkumar, K. V. Sankar, R. K. Selvan, M. Danielle, M. Manickam, Nano α NiMoO4 as a new electrode for electrochemical supercapacitors. RSC Adv, 2013, 3, 352–357.

xxxii. Y. S. Luo, W. D. Zhang, X. J. Dai, Y. Yang and S. Y. Fu, Facile Synthesis and Luminescent Properties of Novel Flowerlike BaMoO4 Nanostructures by a Simple Hydrothermal Route. J. Phys. Chem. C, 2009, 113, 4856-4863. ACS Paragon Plus Environment ACS Applied Materials & 35.

xxxiii. B. Moreno, E. Chinarro, M. T. Colomer, J. R. Jurado, Combustion Synthesis and Electrical Behavior of Nanometric β-NiMoO4. J. Phys. Chem. C, 2010, 114, 4251-4257.

xxxiv. Y. Mi, Z. Y. Huang, F. L. Hu, Y. F. Li, J. Y. Jiang, Room-Temperature Synthesis and Luminescent Properties of Single-Crystalline SrMoO4 Nanoplates. J. Phys. Chem. C, 2009, 113, 20795-20799.

xxxv. W. S. Wang, Y. X. Hu, J. Goebl, Z. D. Lu, L. Zhen, Y. D. Yin, Shape- and Size Controlled Synthesis of Calcium Molybdate Doughnut-Shaped Microstructures. J. Phys. Chem. C, 2009,113, 16414-16423.

xxxvi. Y. Cheng, Y. S. Wang, D. Q. Chen, F. Bao, Evolution of Single Crystalline Dendrites from Nanoparticles through Oriented Attachment. J. Phys. Chem. B, 2005,109, 794-798.

xxxvii. M.K. Xu, Z.H. Ouyang, Z.R. Shen, Topological evolution of cerium(III) molybdate microflake assemblies induced by amino acids. Chin. Chem. Lett, 2016, 27, 673-677.

xxxviii. Tauc, J. (1974) Amorphous and Liquid Semiconductor. Plenium Press, New York.

xxxix. Barve A.K. Gadegone S.M. Lanjewar M.R. Lanjewar R.B. 2014. International journal of Engineering research and applications. ISSN No: 2248-9622.

xl. Md Abdus Subhan, Tanzir Ahmed.Synthesis, characterization and spectroscopic investigations of novel nano multi-metal oxide Co_3O_4-CeO_2-ZnO. Spectrochimica Acta Part A: Molecular and Biomolecular Spectroscopy 129 (2014) 377–381. doi.org/10.1016/j.saa.2014.03.051

xli. Amit Kumar1, Neeraj Kumar Mishra2, Komal Sachan3, Md Asif Ali4, Sachchidanand Soaham Gupta1, Rajeev Singh. Trimetallic oxide nanocomposites of transition metals Titanium and Vanadium by sol-gel technique: Synthesis, characterization and electronic properties. 2018; Mater. Res. Express. https://doi.org/10.1088/2053-1591/aabd23

xlii. J. Song, X. Ni, L. Geo and H. Zheng, Mater. Chem. Phys., 2007, 102, 245–248. of TiO2–ZrO2 and phosphotungstic acid. 2019; J Mater Sci. https://doi.org/10.1007/s10853-019-04144-w.

xliii. Yuehong Song, Yan Zhao, Zhifang Huang, Jingzhe Zhao"Aqueous synthesis of molybdenum trioxide (h-MoO3, α-MoO3·H2O and h-/α-MoO3 composites) and their photochromic properties study",Journal of Alloys and CompoundsVolume 693, 5 February 2017, Pages 1290-1296

xliv. Saisai Yuan, Qitao Zhang, Bin Xu,Zhengyuan Jin, Ya Zhang, Yin Yang, Ming Zhang and Teruhisa Ohno,"Porous cerium dioxide hollow spheres and their photocatalytic performance" RSC Adv., 2014, 4, 62255–62261

xlv. Francesca Scarpelli. Teresa F. Mastropietro. Teresa Poerio and Nicolas Godbert "Mesoporous TiO2 Thin Films: State of the Art" June 2018 DOI:10.5772/intechopen.74244 In book: Titanium Dioxide - Material for a Sustainable EnvironmentPublisher: Submitted: October 19th, 2017Reviewed: January 22nd, 2018Published: June 27th, 2018

xlvi. Brezesinski, T.; Wang, J.; Senter, R.; Brezesinski, K.; Dunn, B.; Tolbert, S. H., On the Correlation between Mechanical Flexibility, Nanoscale Structure, and Charge Storage in Periodic Mesoporous CeO2 Thin Films. ACS Nano **2010,** 4 (2), 967-977.

.